High-temperature Thermoelectric and Microstructural Characteristics of Ga Substituted on the Co-site in Cobalt-based Oxides

Van Nong, Ngo; Yanagiya, S.; Sonne, Monica; Pryds, Nini; Ohtaki, M.

Published in:
Journal of Electronic Materials

Link to article, DOI:
10.1007/s11664-011-1524-1

Publication date:
2011

Journal of ELECTRONIC MATERIALS
DOI: 10.1007/s11664-011-1524-1

High-Temperature Thermoelectric and Microstructural Characteristics of Cobalt-Based Oxides with Ga Substituted on the Co-Site

N.V. NONG,[1,4] S. YANAGIYA,[1,2] S. MONICA,[1] N. PRYDS,[1] and M. OHTAKI[3]

1.—Division of Fuel Cells and Solid State Chemistry, Risø National Laboratory for Sustainable Energy, Technical University of Denmark, 4000 Roskilde, Denmark. 2.—Department of Electrical and Electronic Engineering, Hakodate National College of Technology, 14-1 Tokura, Hakodate, Hokkaido 042-8501, Japan. 3.—Interdisciplinary Graduate School of Engineering Sciences, Kyushu University, Fukuoka 816-8580, Japan. 4.—e-mail: ngno@risoe.dtu.dk

The effects of Ga substitution on the Co-site on the high-temperature thermoelectric properties and microstructure are investigated for the misfit-layered $Ca_3Co_4O_9$ and the complex perovskite-related $Sr_3RECo_4O_{10.5}$ (RE = rare earth) cobalt-based oxides. For both systems, substitution of Ga for Co results in a simultaneous increase in the Seebeck coefficient (S) and the electrical conductivity (σ), and the influence is more significant in the high temperature region. The power factor ($S^2\sigma$) is thereby remarkably improved by Ga substitution, particularly at high temperatures. Texture factor calculations using x-ray diffraction pattern data for pressed and powder samples reveal that the Ga-doped samples are highly textured. Microstructure observed by scanning electron microscopy shows very well-crystallized grains for the samples with Ga substitution for Co. Among the Ga-doped samples, $Ca_3Co_{3.95}Ga_{0.05}O_9$ shows the best ZT value of 0.45 at 1200 K, which is about 87.5% higher than the nondoped one, a considerable improvement.

Key words: Cobalt oxides, hot pressing, electrical conductivity, figure of merit

INTRODUCTION

Cobalt oxides form a large family of compounds with fascinating structural and physical properties. The different possible oxidation states of cobalt (divalent, trivalent, and tetravalent) together with its various spin configurations (for example, low spin, intermediate spin, and high spin) for Co ions are responsible for various interesting phenomena such as temperature-induced spin-state transitions in oxides with perovskite-like structure such as $LaCoO_3$[1] and $Sr_{1-x}Y_xCoO_{3-\delta}$,[2] giant magnetoresistance in $La_{1-x}Sr_xCoO_3$,[3] and unusual thermoelectric properties (coexistence of large thermoelectric power and low electrical resistivity) in the misfit-layered cobalt oxides[4,5] $NaCo_2O_4$ and $Ca_3Co_4O_9$. Many attempts have been made to optimize the thermoelectric performance of these compounds by either ion doping or improving fabrication methods. While most investigations have mainly concentrated on the effects of substitution on the A-site in perovskite-related systems[6–8] or Ca-site in misfit-layered systems,[9–13] a few groups have performed substitution on the Co-site.[14–16] The peculiar structural arrangement of the CoO_6 octahedra, containing cobalt cations with mixed valence of 3+ and 4+, is the origin of the interesting properties of those cobaltites. Ion doping on the Co-sites, especially Co ion in the CoO_6 octahedra isostructural to the CoO_2 planes, possibly induces more notable effects on the transport and thermoelectric properties of these materials as the charge-carrier transport mostly occurs within these layers. Previous reports have shown that substitutions at Co-site by Zr in $(La,Sr)CoO_3$[14] and by Fe in misfit-layered $Ca_3Co_4O_9$[15] are effective in improving the thermoelectric properties of these materials.

(Received May 11, 2010; accepted January 17, 2011)

In this work, the Co-site of the complex perovskite-related $Sr_3RECo_4O_{10.5}$ (RE = Y and Gd) and the misfit-layered $Ca_3Co_4O_9$ cobalt oxides was substituted with Ga. The effects of Ga doping on the microstructure and the high-temperature thermoelectric properties of these systems are systematically investigated and discussed.

EXPERIMENTAL PROCEDURES

Polycrystalline samples of $Ca_3Co_{4-x}Ga_xO_9$ ($0 \le x \le 0.2$) and $Sr_3RECo_{4-x}Ga_xO_{10.5}$ with RE = Y and Gd ($0 \le x \le 0.3$) were synthesized by solid-state reaction from $CaCO_3$, $SrCO_3$, RE_2O_3, Co_3O_4, and Ga_2O_3. Synthesized powders of $Sr_3RECo_{4-x}Ga_xO_{10.5}$ were pressed into pellets under cold isostatic pressure of 250 MPa followed by a sintering process at 1423 K for 24 h after the mixed powders were calcined at 1373 K for 24 h in air. As for the $Ca_3Co_{4-x}Ga_xO_9$ system, the samples after sintering at 1173 K for 48 h with intermediate grinding were reground then hot-pressed into pellets at 1123 K under uniaxial pressure of 60 MPa for 2 h in air. The phase purity was checked by powder x-ray diffraction (XRD) measurements using a Bruker D8 diffractometer with Cu Kα radiation. Structure refinements were analyzed using *Jana*2006 crystallographic software for the powder XRD data. Density of the samples was determined using the Archimedes method. The microstructure of the samples was observed by using a Hitachi scanning electron microscopy (TM-1000) system. The electrical resistivity and thermoelectric power were measured simultaneously from room temperature to 1200 K using an ULVAC-RIKO ZEM3 thermoelectric property measurement system in a low-pressure helium atmosphere. The thermal conductivity was determined from the thermal diffusivity and the specific heat capacity measured from room temperature to 1073 K using LFA-457 laser flash and DSC-404C thermal analysis measurement systems. The carrier concentrations and mobility of samples were measured at room temperature by Hall measurements with applied field of 0.55 T using the van der Pauw method.

RESULTS AND DISCUSSION

XRD analysis at room temperature revealed that nondoped and Ga-doped samples of the $Sr_3RECo_{4-x}Ga_xO_{10.5}$ system are single phase for $x \le 0.1$. However, a small impurity peak could be observed for samples with higher Ga content, e.g., for $x = 0.2$ and 0.3 samples, and the intensity of this peak increased with increasing Ga concentration. As for the $Ca_3Co_{4-x}Ga_xO_9$ system, the structure refinement was analyzed by using *Jana*2006 Rietveld software with input parameters taken from Grebille et al.[17] using the superspace group $X2/m(0, \delta, 0)s0$, which is the standard setting of the superspace group $C2/m(1, \delta, 0)s0$. The calculated and the difference profiles ($R_p = 0.0573$, $R_{wp} = 0.0793$) were found to be in good agreement with previous report,[18] confirming the $Ca_3Co_{4-x}Ga_xO_{9+\delta}$ standard phase. Oxygen content $(9 + \delta)$ was determined through iodometric titration, the δ value being about 0.3 and the difference between samples being less than 1%. Figure 1 shows the result for a typical Ga-doped sample with $x = 0.05$. The lattice constants for the $x = 0$ sample were $a = 4.8347(7)$ Å, $b_1 = 4.5476(9)$ Å, $b_2 = 2.819(1)$ Å, $c = 10.8514(1)$ Å, and $\beta = 98.12(6)°$. The lattice constants determined for the $x = 0.05$ sample were $a = 4.8230(7)$ Å, $b_1 = 4.5467(6)$ Å, $b_2 = 2.807(1)$ Å, $c = 10.8125(3)$ Å, and $\beta = 98.06(2)°$. The structural parameters such as the misfit ratio b_1/b_2, c, and β as indicated by these results are slightly distorted by the Ga doping.

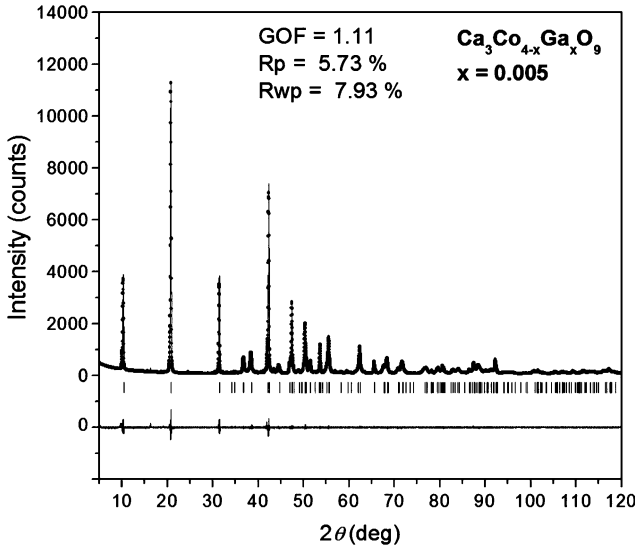

Fig. 1. Observed (dotted line), calculated (solid line), and difference powder XRD profiles ($\lambda = 1.9604$ Å) for the final Rietveld refinement of a typical polycrystalline sample for $Ca_3Co_{4-x}Ga_xO_9$ with $x = 0.05$.

Density of all the samples was measured using the Archimedes method, and the relative densities are listed in Table I. Under the same conditions of pressing and sintering processes, the $Sr_3RECo_4O_{10.5}$ sample with RE = Y exhibited a rather low relative density (65.6%) in comparison with the RE = Gd sample (88.8%). Notably, Ga doping results in a significant increase of the relative density, and the values tend to increase with increasing Ga concentration for the complex perovskite system. As for the layered cobaltite system, the densities of all nondoped and Ga-doped samples were greater than 95%, and their difference was about ≤1.2%. The $Ca_3Co_{4-x}Ga_xO_9$ sample with $x = 0.05$ had the highest relative density value of 96.5%.

Figure 2a–d shows scanning electron microscopy (SEM) images from fractured surfaces for $Sr_3YCo_4O_{10.5}$, $Sr_3YCo_{3.9}Ga_{0.1}O_{10.5}$, $Sr_3GdCo_4O_{10.5}$, and $Sr_3GdCo_{3.9}Ga_{0.1}O_{10.5}$ samples, respectively. Large pores can be clearly observed in the SEM image of $Sr_3YCo_4O_{10.5}$ (Fig. 2a), while the size of the pores is much smaller for the $Sr_3GdCo_4O_{10.5}$ sample

Journal : 11664_JEM | Dispatch : 1-2-2011 | Pages : 7
Article No.: 1524 | ☐ LE ☑ CP | ☐ TYPESET ☑ DISK

Table I. Relative densities and thermoelectric (TE) characteristics of nondoped and Ga-doped samples

Compositions	Relative Density (%)	σ_{300K} (S/cm)	S_{300K} (μV/K)	σ_{1200K} (S/cm)	S_{1200K} (μV/K)
$Sr_3YCo_4O_{10.5}$	65.6	3.6	67.1	126.6	14.3
$Sr_3YCo_{3.9}Ga_{0.1}O_{10.5}$	86.8	24.5	51.9	146.6	17.8
$Sr_3YCo_{3.8}Ga_{0.2}O_{10.5}$	87.3	18.1	23.0	125.4	23.7
$Sr_3YCo_{3.7}Ga_{0.3}O_{10.5}$	88.7	12.6	40.5	113.7	27.1
$Sr_3GdCo_4O_{10.5}$	88.3	3.0	72.7	372.5	14.1
$Sr_3GdCo_{3.9}Ga_{0.1}O_{10.5}$	90.0	11.9	146.8	379.7	32.7
$Ca_3Co_4O_9$	95.3	90.8	136.0	111.0	174.0
$Ca_3Co_{3.95}Ga_{0.05}O_9$	96.5	100.1	140.6	133.6	206.3
$Ca_3Co_{3.9}Ga_{0.1}O_9$	96.0	99.1	140.0	133.0	198.0
$Ca_3Co_{3.8}Ga_{0.2}O_9$	95.8	95.2	155.0	131.0	180.0

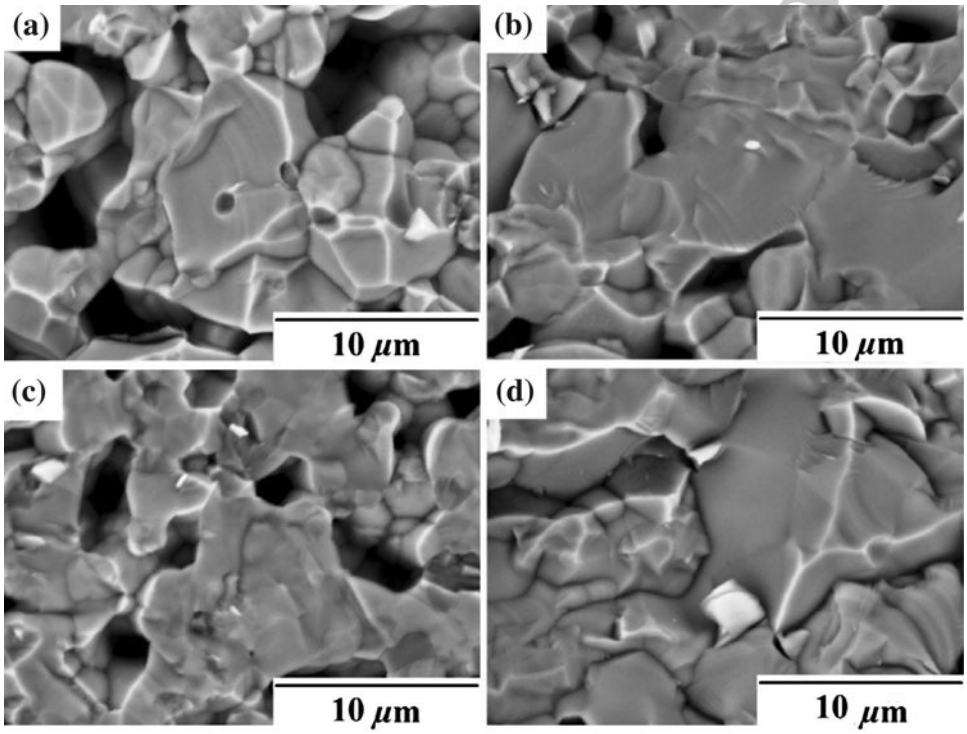

Fig. 2. SEM images from fractured surfaces of the samples for: (a) $Sr_3YCo_4O_{10.5}$, (b) $Sr_3YCo_{3.9}Ga_{0.1}O_{10.5}$, (c) $Sr_3GdCo_4O_{10.5}$, and (d) $Sr_3GdCo_{3.9}Ga_{0.1}O_{10.5}$.

(Fig. 2c). It is also very clear from Fig. 2b, d that the SEM images of the Ga-doped samples show crystalline grains with well-developed crystal faces. This result provides evidence for the difference of relative densities among the samples, as aforementioned. It also suggests that the samples with Ga substitution are highly textured. To elucidate the crystallographic texture, XRD analysis was carried out on a pressed-surface pellet and on free powder. A textured coefficient (TC) for each $(hkl)_i$ reflection can be calculated using the following equation:[19]

$$TC_i = \frac{I_i/I_i^0}{1/n\sum_{i=n} I_i/I_i^0},$$

where I_i is the experimentally determined intensity of the ith reflection for the textured sample, and I_i^0 is the calculated or experimentally determined intensity of the ith reflection from the randomly oriented sample.

Figure 3 shows a comparison between the XRD patterns taken at room temperature for both powder and pressed pellet of a typical $Sr_3GdCo_{3.9}Ga_{0.1}O_{10.5}$ sample and for a pressed pellet of $Sr_3GdCo_4O_{10.5}$. Although the powders which were ground from bulk samples have some degree of crystallinity, the intensities of the XRD peaks of the $Sr_3GdCo_{3.9}Ga_{0.1}O_{10.5}$ sample are much stronger for the pressed surface than for the powders, leading to a textured coefficient of $TC_{33.4°} = 1.92$. These results

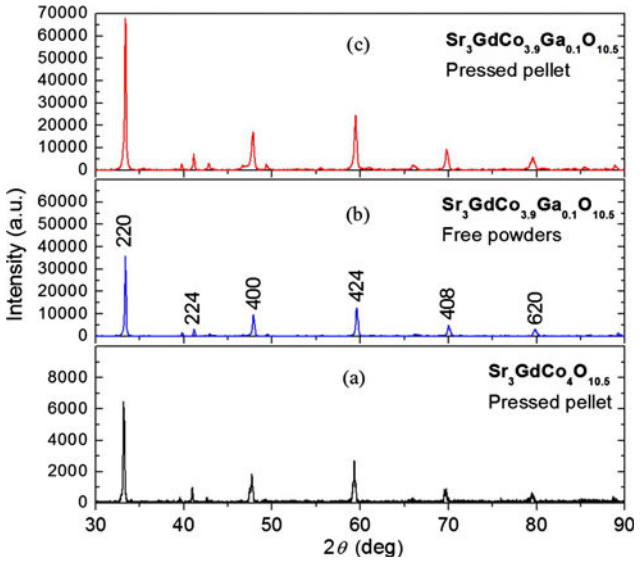

Fig. 3. X-ray diffraction patterns at room temperature for powders and pressed pellets of $Ca_3Co_{4-x}Ga_xO_{10.5}$ samples with $x = 0$ and 0.1.

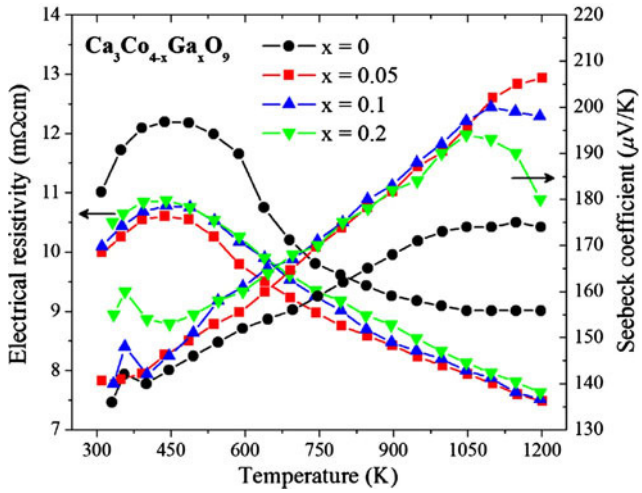

Fig. 5. Temperature dependence of the electrical resistivity and thermoelectric power of $Ca_3Co_{4-x}Ga_xO_{9+\delta}$ samples with $x = 0$, 0.05, 0.1, and 0.2.

are consistent with the microstructure observations above.

Figure 4a–d displays SEM images taken from fractured cross-sections of the misfit-layered $Ca_3Co_{4-x}Ga_xO_9$ system with $x = 0$, 0.05, 0.1, and 0.2, respectively. The fractured cross-sections were taken roughly perpendicular to the pressure direction applied during hot-pressing. A lamella-like structure can be observed in all nondoped and Ga-doped samples, but the grain alignment is more pronounced and better oriented for the Ga-doped ones. SEM images again confirm that all the samples with Ga substitution are highly textured and highly dense, with large crystallographic anisotropy.

Figure 5 shows the temperature dependence of the electrical resistivity and the thermoelectric power for $Ca_3Co_{4-x}Ga_xO_9$ samples with $x = 0$, 0.05, 0.1, and 0.2. It can be seen from Fig. 5 that the ρ–T curve shows metal-like behavior ($d\rho/dT < 0$) below 450 K but nonmetallic behavior ($d\rho/dT > 0$) above

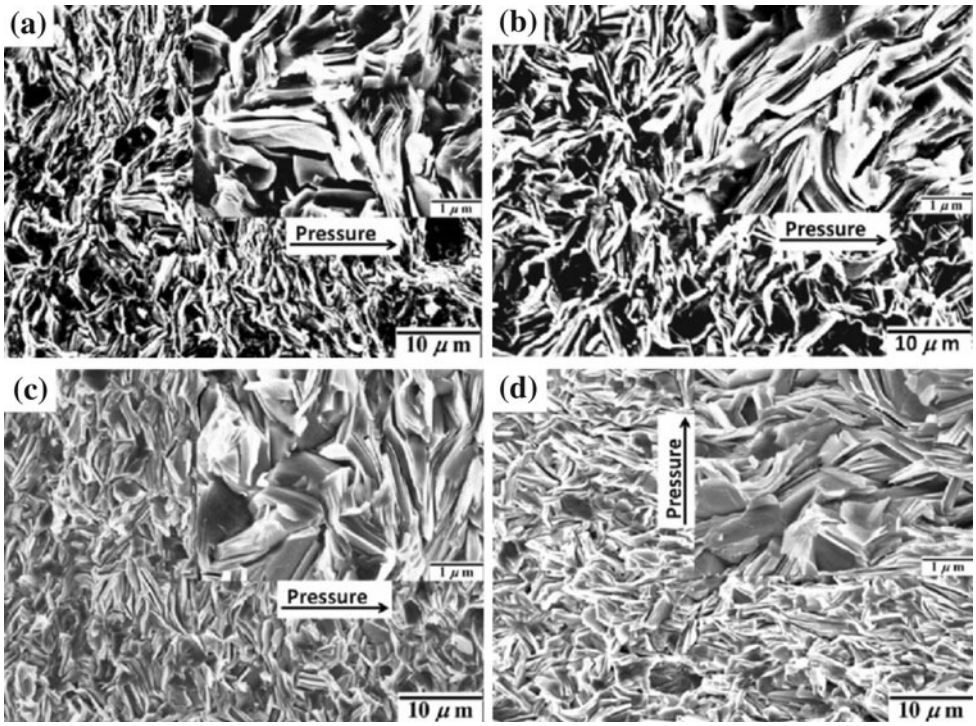

Fig. 4. SEM images of the fractured surfaces roughly perpendicular to the pressure direction of $Ca_3Co_{4-x}Ga_xO_{10.5}$ samples: (a) $x = 0$, (b) $x = 0.05$, (c) $x = 0.1$, and (d) $x = 0.2$.

Journal : 11664_JEM Dispatch : 1-2-2011 Pages : 7
Article No.: 1524 ☐ LE ☑ CP ☐ TYPESET ☑ DISK

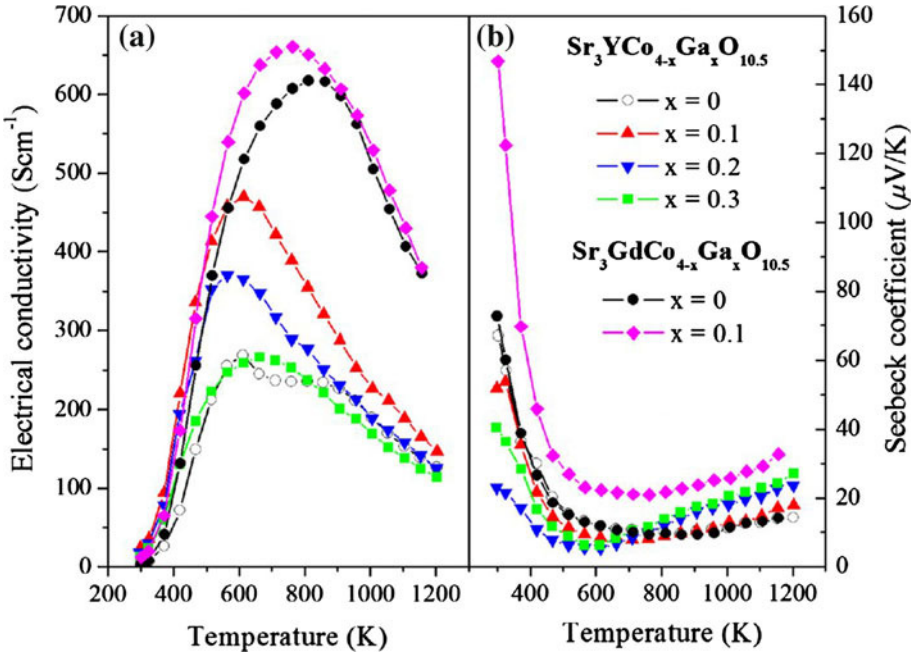

Fig. 6. Temperature dependence of (a) the electrical conductivity, and (b) the thermoelectric power of $Sr_3RECo_{4-x}Ga_xO_{10.5}$ for $0 \le x \le 0.3$ with RE = Y and Gd.

450 K, indicating a metal to insulator (M–I) transition.[13,16] Ga substitution for Co causes a decrease of the electrical resistivity in the whole investigated temperature range. Among the Ga-doped samples, the electrical resistivity tends to increase with increasing Ga concentration for $x > 0.05$. The Seebeck coefficient of all the samples shows positive values over the measured temperature range, indicating a hole conduction mechanism in these compounds. It is also clear that substitution of Ga for Co results in an increase in the thermoelectric power, and the effect is more significant in the high temperature region ($T > 600$ K). However, S decreases with increasing Ga concentration for $x > 0.05$ in the temperature region $T > 1050$ K.

Temperature dependence of the electrical conductivity and the Seebeck coefficient of nondoped and Ga-doped $Sr_3RECo_{4-x}Ga_xO_{10.5}$ with RE = Y and Gd are shown in Fig. 6a, b, respectively. In general, σ–T curves of the samples increase with increasing temperature, and they decrease rapidly after reaching a maximum at around $T_{cusp} = 650 \pm 5$ K and 810 ± 5 K for the samples with RE = Y and Gd, respectively. As is also clearly seen from Fig. 6a, the σ values of the Ga-doped samples are higher than the nondoped one, particularly for the $x = 0.1$ samples, and the T_{cusp} tends to shift to lower temperature. This would be related to the influence of the Ga doping at the Co-site. Among the Ga-doped samples, σ tends to decrease with increasing Ga concentration for $x > 0.1$. A possible reason may be due to the fact that the samples with higher Ga content (e.g., for $x = 0.2$ and 0.3) contain a secondary phase. In contrast to the electrical conductivity, the Seebeck coefficient, which also shows p-type conduction, dramatically decreases with increasing temperature, and it takes a concave shape at temperature that corresponding to the T_{cusp} of the σ–T curves. It then increases gradually with further increase of the temperature. The Seebeck coefficient shows a larger value at higher concentration of Ga substitution for Co in the temperature range of $T > 700$ K. The σ and S values of all the nondoped and Ga-doped samples from 300 K and 1200 K are listed in Table I, showing that substitution of Ga for Co for $x \le 0.1$ results in an increase of both the electrical conductivity and the Seebeck coefficient of the samples at high temperatures. In general, the increase in the electrical conductivity due to the increase of the carrier concentration will also result in a decrease of the thermoelectric power. The simultaneous increase of the electrical conductivity and the thermoelectric power for the Ga-doped samples suggests that such a phenomenon cannot be explained by the above-mentioned general relationship between S and σ. However, the energy-correlated carrier mobility $\mu(E)$ may play a crucial role in determining S. According to Ref. 20, the Seebeck coefficient can be expressed by the following formula:

$$S(T) = \frac{c_e}{n} + \frac{\pi^2 \kappa_B^2 T}{3e}\left[\frac{\partial \ln \mu(E)}{\partial E}\right]_{E=E_F}, \qquad (1)$$

where $c_e = (\pi^2 k_B^2 T/3e)N(E)$, and n, c_e, k_B, and $N(E)$ are the carrier concentration, specific heat, Boltzmann constant, and density of states, respectively. Although the first term c_e/n of Eq. 1 is inversely

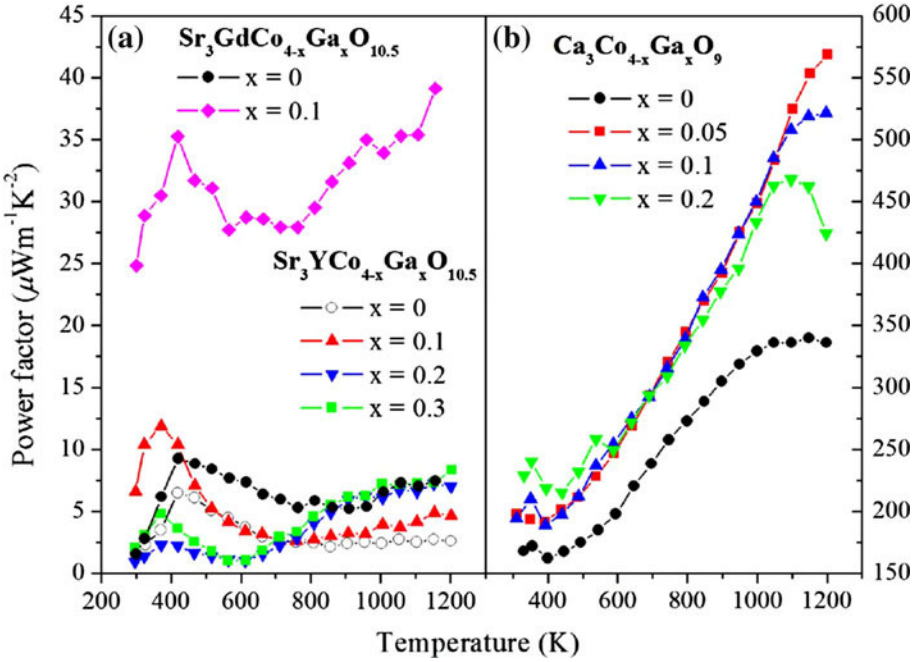

Fig. 7. Temperature dependence of the power factor for: (a) $Sr_3RECo_{4-x}Ga_xO_{10.5}$ with $0 \le x \le 0.3$ with RE = Y and Gd, and (b) $Ca_3Co_{4-x}Ga_xO_{9+\delta}$ with x = 0, 0.05, 0.1, and 0.2.

proportional to the carrier concentration, the increase of thermoelectric power at high temperature for the Ga-doped samples suggests that the second term may play a dominant role in determining S for these materials at high temperatures. We could assume that Ga doping for Co occurs at the Co-site having mixed valence of Co^{3+}/Co^{4+}, in which transport properties are dominated by holes. This causes a change in $\mu(E)$, and this change affects the increase of S. Unfortunately, we have not yet obtained data for $\mu(E)$ from Hall measurements at high temperature. However, evidence from Hall measurements for the Ga-doped $Ca_3Co_{4-x}Ga_xO_9$ system at room temperature revealed that the carrier concentration n and μ increased from 1.97×10^{20} cm^{-3} and 0.67 $cm^2/V\,s$ for the nondoped sample to 2.34×10^{20} cm^{-3} and 1.56 $cm^2/V\,s$ for the Ga-doped sample with $x = 0.05$, respectively. Moreover, a possible reason for why Ga substitutes for Co in the aforementioned Co-site may also stem from their different ionic radii. Considering the usual spin states of these cations, the radius of Ga^{3+} (0.62 Å) is close to that of Co^{3+} (0.545 Å/0.61 Å, low-spin/high-spin states) and Co^{4+} (0.53 Å, low-spin state),[21] so Co^{3+}/Co^{4+} ions can be substituted by the Ga ion. The larger ionic radius of Ga^{3+} substitution for Co causes distortion of the structure and hence has a notable effect on carrier transport. However, since the ionic radius of Ga^{3+} is larger when compared with Co^{3+}/Co^{4+}, substitution of Ga for Co becomes more difficult with increasing Ga content. This may explain why the Ga-doped $Sr_3RECo_{4-x}Ga_xO_{10.5}$ system for $x \ge 0.2$ showed an impurity phase. As for the $Ca_3Co_{4-x}Ga_xO_9$ system, σ and S tended to decrease with higher Ga concentration for $x > 0.05$, e.g., $x = 0.1$ and 0.2. In this case Ga^{3+} might substitute for Co^{4+}, causing a decrease in the Co^{4+}/Co^{3+} ratio, leading to the decrease of hole concentration.

As a net result of the simultaneous increase of thermoelectric power and electrical conductivity, the power factor is significantly improved by Ga substitution, as shown in Fig. 7a, b for the complex perovskite and layered-cobalt systems, respectively. The power factor is about 40 $\mu W/mK^2$ attained for the $Sr_3GdCo_{4-x}Ga_xO_{10.5}$ with $x = 0.1$, compared with 8 $\mu W/mK^2$ for the nondoped sample at 1200 K. Note that, for the $Ca_3Co_{4-x}Ga_xO_9$ system, the power factor of the $x = 0.05$ sample at 1200 K is 570 $\mu W/mK^2$, which is about 1.7 times larger than that of the nondoped sample. As for the compositions with $x = 0.1$ and 0.2, the power factor seems to reach a maximum value at a temperature of 1100 K, while the maximum power factor of the $x = 0.05$ sample has not yet been reached within this range of temperatures.

To determine the figure of merit for the Ga-doped layered-cobalt system, the thermal conductivity (κ) of the nondoped and Ga-doped, $x = 0.05$ samples were measured and are presented in Fig. 8. For both samples, κ decreases with increasing temperature, and the values are somewhat lower for the Ga-doped sample than for the nondoped one, particularly in the high temperature region ($T > 400$ K). Thermal conductivity (κ_{total}) can be expressed by the sum of a lattice component (κ_{ph}) and an electronic component (κ_e) as $\kappa_{total} = \kappa_{ph} + \kappa_e$. In this case, the contribution of κ_e to κ_{total}, estimated from the Wiedemann–Franz relation, is small,

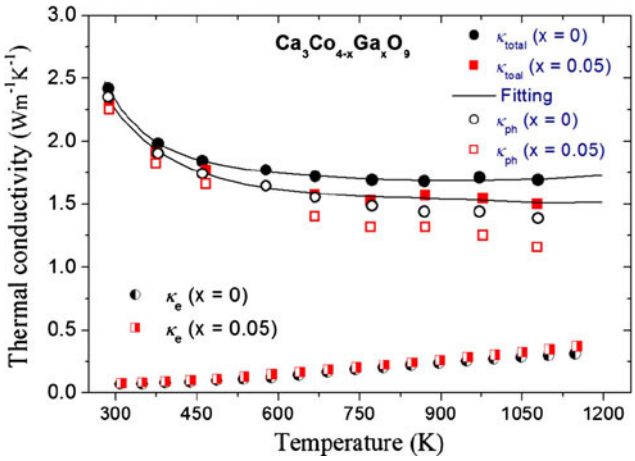

Fig. 8. Electronic and phonon contributions (κ_e and κ_{ph}) to the thermal conductivity (κ_{total}) of $Ca_3Co_{4-x}Ga_xO_9$ with $x = 0$ and 0.05 as a function of temperature.

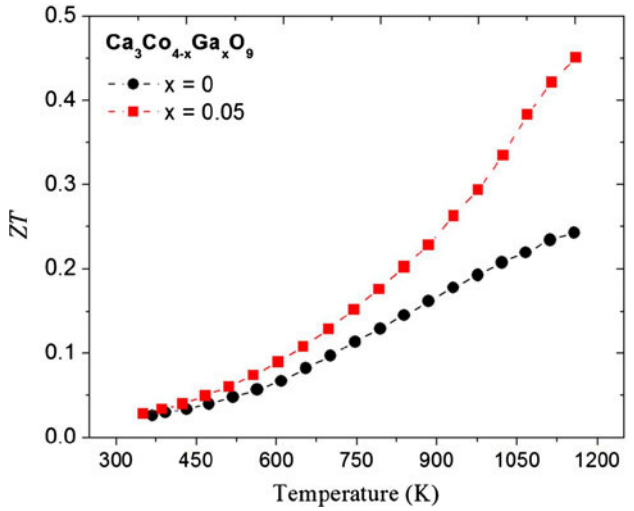

Fig. 9. The dimensionless figure of merit (ZT) of $Ca_3Co_{4-x}Ga_xO_9$ with $x = 0$ and 0.05 as a function of temperature.

indicating the major contribution of the phonon term κ_{ph}, as clearly shown in Fig. 8. The decrease in κ_{total} is therefore attributed to the reduction of lattice component due to incorporation of heavier Ga^{3+} compared with Ca^{2+} ions. Figure 9 presents the dimensionless figure of merit, ZT, versus temperature for the $x = 0$ and $x = 0.05$ samples, showing that ZT is significantly improved, particularly in the high temperature region. The ZT value of the $x = 0.05$ samples could reach 0.45 at about 1200 K.

CONCLUSIONS

We have investigated the effects of Ga substitution on the Co-site on the high-temperature thermoelectric (TE) properties and microstructure of a series of samples for the complex perovskite $Sr_3RECo_{4-x}Ga_xO_{10.5}$ (RE = Y and Gd) for $0 \le x \le 0.3$ and the misfit-layered $Ca_3Co_{4-x}Ga_xO_9$ ($0 \le x \le 0.2$) systems. Substitution of Ga resulted in simultaneously increase of the electrical conductivity and the thermoelectric power. This effect is more significant in the high temperature region. Observation of the microstructure indicated that Ga could act as a sintering aid, which clearly enhanced crystallographic texture, leading to higher density of the samples. The thermoelectric power factor was effectively improved by partial Ga substitution, particularly for the $Sr_3GdCo_{3.9}Ga_{0.1}O_{10.5}$ and $Ca_3Co_{3.95}Ga_{0.05}O_9$ samples. A maximum ZT value of about 0.45 could be obtained for $Ca_3Co_{3.95}Ga_{0.05}O_9$ at 1200 K, suggesting a promising oxide material for power generation from high-temperature waste heat.

REFERENCES

1. P.M. Raccah and J.B. Goodenough, *Phys. Rev.* 155, 932 (1967). doi:10.1103/PhysRev.155.932.
2. S. Kimura, Y. Maeda, K. Kashiwagi, H. Yamaguchi, M. Hagiwara, S. Yoshida, I. Terasaki, and K. Kindo, *Phys. Rev. B* 78, 180403 (2008). doi:10.1103/PhysRevB.78.180403.
3. G. Briceno, H. Chang, X. Sun, P.G. Schultz, and X.D. Xiang, *Science* 270, 273 (1995).
4. I. Terasaki, Y. Sasago, and K. Uchinokura, *Phys. Rev. B* 56, R12685 (1997). doi:10.1103/PhysRevB.56.R12685.
5. M. Shikano and R. Funahashi, *Appl. Phys. Lett.* 82, 1851 (2003). doi:10.1143/JJAP.45.4152.
6. T. He, J. Chen, T.G. Calvarese, and M.A. Subramanian, *Solid State Sci.* 8, 467 (2006). doi:10.1016/j.solidstatesciences.2006.01.002.
7. S. Yoshida, W. Kobayashi, T. Nakano, I. Terasaki, K. Matsubayashi, Y. Uwatoko, I. Grigoraviciute, M. Karppinen, and H. Yamauchi, *J. Phys. Soc. Jpn.* 78, 094711 (2009). doi:10.1143/JPSJ.78.094711.
8. J.W. Moon, Y. Masuda, W.S. Seo, and K. Koumoto, *Mater. Lett.* 48, 225 (2001).
9. Y. Wang, Y. Sui, J. Cheng, X. Wang, J. Miao, Z. Liu, Z. Qian, and W. Su, *J. Alloys Compd.* 448, 1 (2008). doi:10.1016/j.jallcom.2006.10.047.
10. F.P. Zhang, Q.M. Lu, and J.X. Zhang, *Phys. B* 404, 2142 (2009). doi:10.1016/j.physb.2009.04.002.
11. M. Prevel, E.S. Reddy, O. Perez, W. Kobayashi, I. Terasaki, C. Goupil, and J.G. Noudem, *Jpn. J. Appl. Phys.* 46, 6533 (2007). doi:10.1143/JJAP.46.6533.
12. H.Q. Liu, X.B. Zhao, T.J. Zhu, Y. Song, and F.P. Wang, *Curr. Appl. Phys.* 9, 409 (2009). doi:10.1016/j.cap.2008.03.010.
13. D. Wang, L. Cheng, Q. Yao, and J. Li, *Solid State Commun.* 129, 615 (2004). doi:10.1016/j.ssc.2003.11.045.
14. Y. Fujine, H. Fujishiro, K. Suzuki, Y. Kashiwada, and M. Ikebe, *J. Magn. Magn. Mater.* 272–276, 104 (2004). doi:10.1016/j.jmmm.2003.11.045.
15. C.J. Liu, L.C. Huang, and J.S. Wang, *Appl. Phys. Lett.* 89, 204102 (2006). doi:10.1063/1.2390666.
16. Y. Wang, Y. Sui, X. Wang, W. Su, and X. Liu, *J. Appl. Phys.* 107, 033708 (2010). doi:10.1063/1.3291125.
17. D. Grebille, S. Lambert, F. Bouree, and V. Petricek, *J. Appl. Crystallogr.* 37, 823 (2004). doi:10.1107/S0021889804018096.
18. C.D. Ling, K. Aivazian, S. Schmid, and P. Jensen, *J. Solid State Chem.* 180, 1446 (2007). doi:10.1016/j.jssc.2007.02.016.
19. M.H. Mueller, W.P. Chernock, and P.A. Beck, *Trans. Metall. Soc. AIME* 212, 39 (1958).
20. G. Xu, R. Funahashi, M. Shikano, Q. Pu, and B. Liu, *Solid State Commun.* 124, 73 (2002). doi:10.1016/S0038-1098(02)00495-7.
21. R.D. Shanon, *Act. Cryst.* A32, 751 (1976). doi:10.1107/S0567739476001551.